Diffusion tensor tractography in children with sensory processing disorder: Potentials for devising machine learning classifiers☆

Seyedmehdi Payabvash[a,b], Eva M. Palacios[b], Julia P. Owen[c], Maxwell B. Wang[b], Teresa Tavassoli[d], Molly Gerdes[e], Anne Brandes-Aitken[f], Elysa J. Marco[e,g], Pratik Mukherjee[b,h,*]

[a] Department of Radiology and Biomedical Imaging, Yale School of Medicine, New Haven, CT, United States of America
[b] Department of Radiology and Biomedical Imaging, University of California, San Francisco, CA, United States of America
[c] Department of Radiology, University of Washington, Seattle, WA, United States of America
[d] Department of Psychology and Clinical Sciences, University of Reading, Reading, United Kingdom
[e] Department of Neurology, University of California, San Francisco, CA, United States of America
[f] Department of Applied Psychology, New York University, New York, NY, United States of America
[g] Department of Pediatric Neurology, Cortica Healthcare, San Rafael, CA, United States of America
[h] Department of Bioengineering and Therapeutic Sciences, University of California, San Francisco, CA, United States of America

ARTICLE INFO

ABSTRACT

The "sensory processing disorder" (SPD) refers to brain's inability to organize sensory input for appropriate use. In this study, we determined the diffusion tensor imaging (DTI) microstructural and connectivity correlates of SPD, and apply machine learning algorithms for identification of children with SPD based on DTI/tractography metrics. A total of 44 children with SPD and 41 typically developing children (TDC) were prospectively recruited and scanned. In addition to fractional anisotropy (FA), mean diffusivity (MD), and radial diffusivity (RD), we applied probabilistic tractography to generate edge density (ED) and track density (TD) from DTI maps. For identification of children with SPD, accurate classification rates from a combination of DTI microstructural (FA, MD, AD, and RD), connectivity (TD) and connectomic (ED) metrics with different machine learning algorithms – including naïve Bayes, random forest, support vector machine, and neural networks – were determined. In voxel-wise analysis, children with SPD had lower FA, ED, and TD but higher MD and RD compared to TDC – predominantly in posterior white matter tracts including posterior corona radiata, posterior thalamic radiation, and posterior body and splenium of corpus callosum. In stepwise penalized logistic regression, the only independent variable distinguishing children with SPD from TDC was the average TD in the splenium (p < 0.001). Among different combinations of machine learning algorithms and DTI/connectivity metrics, random forest models using tract-based TD yielded the highest accuracy in classification of SPD – 77.5% accuracy, 73.8% sensitivity, and 81.6% specificity. Our findings demonstrate impaired microstructural and connectivity/connectomic integrity in children with SPD, predominantly in posterior white matter tracts, and with reduced TD of the splenium of corpus callosum as the most distinctive pattern. Applying machine learning algorithms, these connectivity metrics can be used to devise novel imaging biomarkers for neurodevelopmental disorders.

1. Introduction

Sensory processing disorder (SPD) is a clinical condition, referring to challenges in modulation and organization of sensory input for appropriate use (Miller et al., 2007; Mitchell et al., 2015). It is estimated that up to 16% of children in the United States are affected by SPD (Ahn

---

et al., 2004; Ben-Sasson et al., 2009). Children with SPD often have problems with skills and abilities required for academic success in school. Due to the disruptions in sensory processing, many children with SPD also demonstrate delayed or atypical developmental language and motor milestones, which become more apparent over time with more complex and rapid tasks (May-Benson et al., 2009). As a result, children with SPD often suffer from emotional, social, and educational challenges, including anxiety, aggression, inattention, poor self-concept, dysgraphia, and academic failure (Miller et al., 2009). Moreover, children with atypical sensory modulation such as hyper- or hypo-responsivity to sound or touch may also meet criteria for other behavioral conditions such as autism spectrum disorder (ASD) and attention deficit hyperactivity disorder (ADHD) (Koziol and Budding, 2012; Tomchek and Dunn, 2007). While most children with SPD do not have social communication challenges that meet criteria for ASD, up to 92% of patients with ASD suffer from hyper- or hypo-responsivity (Tomchek and Dunn, 2007). Furthermore, symptoms of ADHD are often present in SPD, with over 40% of children with SPD presenting with prominent inattention and/or hyperactivity (Brandes-Aitken et al., 2018; Koziol and Budding, 2012). Up until recently, SPD was not recognized as a brain-based condition; thus, confirmation of a behavioral diagnosis with an objective biomarker is important step for a better understanding and categorization of the condition. As we continue to search for better means of characterization and diagnosing sensory-based challenges, we can treat the root of the dysfunction rather than downstream behavioral consequences such as prominent oppositional behavior (Chang et al., 2014). It is therefore crucial to define the neural underpinnings of this increasingly recognized neurodevelopmental condition, and devise objective biomarkers for identification and prognostication.

Prior DTI studies in a small cohort of children with SPD revealed impaired white matter microstructure predominantly in the posterior projection and commissural tracts with decreased fractional anisotropy (FA) and increased radial diffusivity (RD) (Chang et al., 2015; Owen et al., 2013). While these conventional DTI measures of water diffusivity are used as a proxy for white matter connectivity and integrity, they represent spatially averaged properties over voxels, and include many discrete, and often opposing, directional components (Mukherjee et al., 2008a,b). By contrast, probabilistic tractography applies streamline construction of diffusion fiber tracks with attention to the directionality of water molecule movements, and thus constructs track density (TD) maps, which may provide new perspective regarding underlying white matter microstructural changes (Calamante et al., 2010, 2012a,b). The complex network of neuronal connections in human brain can also be studied using graph theory, with cortical and subcortical gray matter regions represented by "nodes", and the interconnecting white matter pathways by "links" or "edges" (Bullmore and Sporns, 2009). Edge density (ED) imaging offers a framework to represent the spatial anatomic embedding of such connectomic edges within the white matter (Greene et al., 2017; Owen et al., 2015).

In order to fully characterize the neural circuitry correlates of SPD, we applied a voxel-wise analysis to examine the diffusion properties of white matter using conventional DTI metrics including FA, RD, mean diffusivity (MD), and axial diffusivity (AD). Next, by applying probabilistic tractography, we generated TD and ED maps to compare the white matter connectivity in children with SPD versus typically developing children (TDC). Then, we applied stepwise penalized logistic regression to identify the independent predictor(s) of SPD among tract-based DTI microstructural and connectivity metrics, which can illuminate the most distinctive pattern of white matter changes in children with broadly defined SPD and has the potential to serve as a region-of-interest (ROI) –based diagnostic tool. Finally, we test the feasibility of machine learning classifiers in devising novel imaging biomarkers for SPD – integrating a multitude of topographic DTI microstructural and connectomic inputs. We present the comparative results, combining different supervised machine learning algorithms with tract-based DTI microstructural and connectivity metrics.

2. Methods

2.1. Subjects

Children aged 8 to 12 years were prospectively recruited through UCSF Sensory Neurodevelopment and Autism Program. Exclusion criteria included positive screening for ASD using the social communication questionnaire (Rutter et al., 2003), history of premature birth, and presence of a psychiatric, genetic, or neurologic diagnosis on interview. The research designation of SPD was based on scores on the "Definite Difference" range for at least one section of the parent report Sensory Profile (Chang et al., 2014, 2015; Owen et al., 2013). The TDC were recruited from the community, and were screened to rule out ASD and SPD. The study design was approved by the Institutional Review Board. Written, informed consents/assents from primary caregivers/study participants were obtained.

2.2. Image acquisition protocol

Brain scans were performed using a 12-channel head coil on a 3-Tesla MRI scanner (Siemens, Tim Trio, Erlangen, Germany). Whole brain DTI scans were acquired using a diffusion-weighted echoplanar sequence with Echo Time = 8000 ms; Time to Repeat = 109 ms; field of view = 220 mm; voxel size = $2.2 \times 2.2 \times 2.2$ mm; 64 diffusion directions at b value of 2000 s/mm^2; and one image with b value of 0 s/mm^2. The T1-weighted images were obtained using 3-dimensional magnetization-prepared rapid acquisition gradient echo for anatomical registration (Echo Time = 2.98 ms, Time to Repeat = 2300 ms, inversion time = 900 ms, flip angle = 9°) (Chang et al., 2014, 2015; Owen et al., 2013).

2.3. DTI post-processing

The FSL 5.0.8 (Oxford, UK) software was used for image post-processing; and all steps have been described previously (Chang et al., 2015; Chang et al., 2014; Owen et al., 2015; Payabvash et al., 2019a,b). First, the brain tissue was extracted using the Brain Extraction Tool (BET) from FSL. Then, the Diffusion Toolbox in FSL (DTIFIT) was used for preliminary data check, and to confirm that the principal eigenvectors (V1) are correctly oriented. Afterwards, TOPUP and EDDY functions from FSL were consecutively applied to correct for susceptibility-induced distortion, eddy currents, and subject motion. After these corrections, the FTIFIT was applied on corrected diffusion scans to generate FA, MD, RD, and AD maps. The BEDPOSTX tool was applied to estimate diffusion parameters at each voxel, and modeling multiple fiber orientations per each voxel (Chang et al., 2014, 2015; Owen et al., 2015). The BEDPOSTX toolbox automatically determines the number of crossing fiber at each voxel; applying the default recommendations from software, the number of fibers modelled per each voxel was set to 2, with multiplicative "weight" factor of 1, and 1000 "burn in" iterations. For TD maps, probabilistic tractography was performed using probtrackx2 with 5000 streamlines initiated from each white matter voxel (Owen et al., 2015). For edge density imaging (EDI), 82 cortical and subcortical regions were extracted from T1-weighted images using Freesurfer 5.3.0 (Massachusetts General Hospital, Boston, MA), and then registered to diffusion space serving as seed/target regions (connectome nodes) for probabilistic tractography (Greene et al., 2017; Owen et al., 2015). The FA maps were first registered to the structural T1-weighted image by linear affine transformation; then the reverse matrix was used for registration of seed/target regions to original diffusion space. The total number of connectome edges passing through each voxel was calculated as the ED value for that voxel (Greene et al., 2017; Owen et al., 2015).

2.4. Voxel-wise analysis

The FSL Tract-Based Spatial Statistics (TBSS) was used for coregistration and voxel-wise comparison of DTI microstructural and connectivity metrics (Owen et al., 2013). As per software recommendations, all FA maps were aligned to every other one to identify the "most representative" map, which was then used as the target image. This target FA map was then affine-aligned into MNI152 standard space. Then all other FA maps were transformed into MNI152 space by combining the nonlinear transform to the target map with the affine transform from that target to MNI152 space (Payabvash et al., 2019b). We also applied Voxel-based morphometry (VBM) to evaluate for voxel-wise differences in focal gray matter volume/topography between two study groups (Douaud et al., 2007; Smith et al., 2004). The FSL "Randomise" tool was used for voxel-wise comparison of study groups, applying 5000 nonparametric permutations, and threshold-free cluster enhancement (TFCE) for family-wise error correction. The age and gender were included as covariates in General Linear Model (GLM) constructs.

2.5. Statistics and machine learning algorithms

The continuous, and nominal variables were compared with Student t and Fisher's exact t-tests, respectively. Using the matrixes from TBSS coregistration step for inverse spatial transformation of JHU ICBM-DTI-81 template to native diffusion space, the average DTI and tractography metrics of 48 white matter tracts were extracted and used as input for stepwise penalized logistic regression and machine learning algorithms. The scatter plot distribution of tract-based average TD and ED values for select 8 white matter tracts, along with independent t-test comparison, and Cohen's d effect size were determined using the "effsize" package from "R". For penalized logistic regression analysis, we used the "stepPlr" package from "R" applying forward and backward stepwise variable selection without interaction. Different supervised machine learning algorithms were applied for classification of children with SPD, including naïve Bayes, random forest, support vector machine (SVM), and neural networks. Similar to radiomics analysis methodology, and given the high-throughput data-mining nature of our analysis, feature selection was applied to reduce overfitting of models and increase the generalizability (Parmar et al., 2015). For feature selection among DTI/tractography metrics, we only included the top 10 tract-based variables with the greatest area under the curve (AUC) in receiver operating characteristics (ROC) analysis for prediction of children with SPD. Notably, our preliminary results showed improvement in average accuracy of predictive models in cross validation after application of feature selection. For naïve Bayes, we applied the "naivebayes" package with a Laplace smoothing value of 0. For random forest, we applied the "randomForest" package with 500 random trees in each model and a randomly selected one-third subset of variables tried at each split. For SVMs, we applied the "e1071" package using a linear kernel with a cost of 0.1, and a polynomial kernel with a sigma of 1. For neural networks, we applied the "neuralnet" using a single hidden layer network with 3 nodes, and double hidden layer network with 3 nodes in the first layer and 2 nodes in the second layer. For cross-validation of each machine learning algorithm, subjects were randomly split into training and validation samples with 4:1 ratio for 500 iterations; and the average (95% confidence interval) of test characteristics were calculated among 500 validation samples using confusion matrix – i.e., classification accuracy, sensitivity, specificity, positive predictive value (PPV), and negative predictive value (NPV). All statistical analysis was performed using the R free software (https://cran.r-project.org/).

Table 1
Subjects characteristics.

	SPD (n = 44)	TDC (n = 41)	P value
Age (years)	9.6 ± 1.8	10.2 ± 1.9	0.139
Gender (girl)	14/44 (32%)	9/41 (22%)	0.338
Perceptual Reasoning Index	115.2 ± 11.3	113.2 ± 13.9	0.467
Verbal Comprehension Index	118.2 ± 12.8	119.2 ± 12.5	0.717
Working Memory Index	105.2 ± 13.1	108.9 ± 10.9	0.162
Processing Speed Index	97.2 ± 12.9	101.1 ± 13.5	0.177

3. Results

3.1. Participants' characteristics

A total of 44 children with SPD, and 41 TDC were included in this study. Table 1 summarizes the subjects' demographic characteristics. There was no significant difference between children with SPD and TDC with regards to age, gender ratio, or general cognitive performance. Nevertheless, age and gender were included as covariates in the voxel-wise statistical analysis to account for any within-group or between-group variation due to axonal development or sex.

3.2. White matter microstructural and connectomic changes in children with SPD

The TBSS voxel-wise analysis of DTI microstructural metrics revealed lower FA but higher MD and RD in children with SPD compared to TDC, throughout much of the white matter. In voxel-wise analysis of DTI tractography connectivity metrics, children with SPD had lower ED and TD compared to TDC, throughout much of the white matter. Fig. 1 shows that the posterior white matter tracts, including posterior corona radiata, posterior thalamic radiation, and posterior body and splenium of the corpus callosum, had the greatest voxel-wise differences between the two study groups. There was no significant difference in AD between the two study groups. In GLM analysis, patient's age and gender had no significant effect on voxel-wise TBSS results.

Table 2 also lists white matter tracts with significant voxel-wise difference in DTI microstructural and connectivity metrics comparing children with SPD and TDC groups. The scatterplots in Fig. 2 depicts the distribution and Cohen's d effect size of average TD and ED among eight white matter tracts comparing SPD and TDC.

In multivariable stepwise penalized logistic regression model, among all tract-based DTI microstructural and connectivity metrics, the only independent variable distinguishing children with SPD from TDC is the average TD in splenium of corpus callosum (p < .001). The ROC AUC for the average TD of corpus callosum splenium in identifying children with SPD was 0.692 (95% confidence interval: 0.579 to 0.804, p = .002).

3.3. Gray matter macrostructural analysis

The VBM analysis showed no significant voxel-wise difference in regional volume or morphometry of the gray matter in SPD versus TDC. In GLM constructs, patients' age and gender also revealed no significant difference in voxel-wise analysis comparing the two study groups.

3.4. Applying machine learning algorithms for classification of SPD

Fig. 3 and Supplemental Table 1 summarize the cross-validation performance for combination of different machine learning algorithms with DTI microstructural and connectivity metrics in classification of children with SPD after 500 iterations. Overall, the models using TD and ED had greater accuracy, sensitivity, specificity, PPV, and NPV, when compared to those using FA, MD, or RD. With regard to different machine learning methods, the naïve Bayes and random forest models
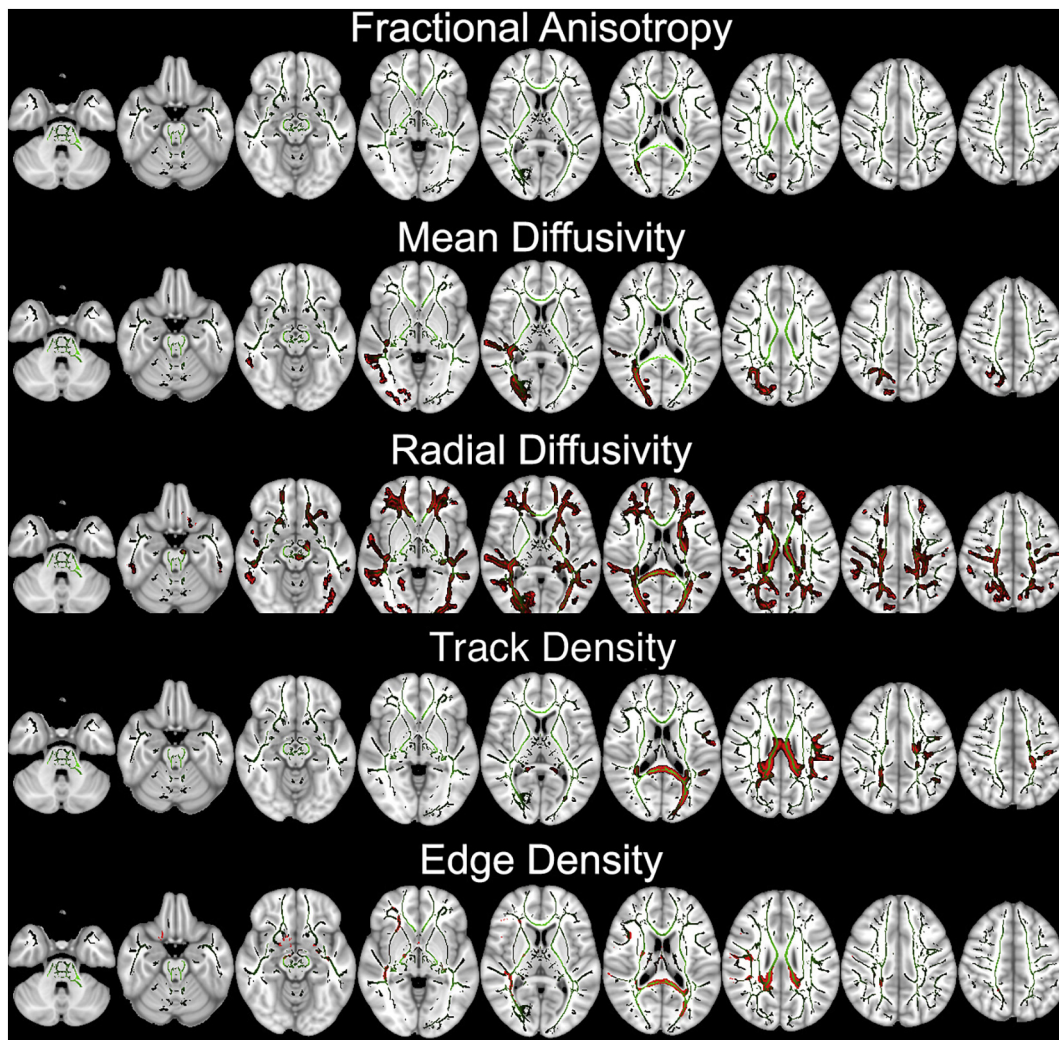
Fig. 1. The results of TBSS voxel-wise analysis: children with SPD had lower FA, TD, and ED but higher MD and RD compared to TDC. The mean skeletonized FA is overlaid on MNI-152 brain map in green color; and white matter tracks with significant voxel-wise difference after applying TFCE correction, are filled with red. (For interpretation of the references to color in this figure legend, the reader is referred to the web version of this article.)

demonstrate better classification performance. Overall, the combination of random forest and tract-based TD had greater accuracy, sensitivity, specificity, PPV, and NPV compared to other combinations – 77.5%, 73.8%, 81.6%, 82.7%, and 74.7%, respectively.

4. Discussion

This study represents the first exploration of the white matter microstructural and connectivity correlates for SPD. We found extensive microstructural impairment manifested by lower FA and increased MD and RD in anterior and posterior white matter tracts. In addition, children with SPD compared to TDC, had lower density of probabilistic fiber tracks and connectomic edges passing through posterior white matter pathways, with the greatest difference at the splenium of the corpus callosum. Notably, among different tract-based DTI microstructural and connectivity metrics, the average TD of the corpus callosum splenium was the only independent predictor for SPD. This finding not only highlights the crucial role of splenial microstructure and connectivity in the neurobiology of SPD, but also offers an ROI-based tool for diagnosis of children with SPD, which can potentially be incorporated in clinical interpretation of brain scans in children with suspected neurodevelopmental disorders. However, further studies are needed to determine whether this ROI-based biomarker can also discriminate children with SPD from those with other neurodevelopmental

conditions, given considerable phenotypic and neural co-morbidity. Finally, our comparative study of supervised machine learning algorithms demonstrates the feasibility of these models for objective and accurate classification of children with SPD based on a multitude of topographic microstructural and connectivity data extracted from DTI scans. Although future studies should aim at teasing out the connectomic-based machine learning classifiers distinguishing children with SPD from those with other neurodevelopmental disorders, such as ASD.

This study extends our previous neuroimaging work in children with SPD showing impaired white matter microstructure, predominantly involving the posterior cerebral tracts using conventional DTI metrics (Chang et al., 2014, 2015; Owen et al., 2013). In 2013, comparing 16 boys with SPD and 24 TDC, Owen et al. found disrupted microstructural integrity primarily in posterior white matter as well as strong correlations between the FA and RD of these tracts with atypical unimodal and multisensory integration behavior (Owen et al., 2013). In 2014, Chang et al. showed that children with SPD and ASD have decreased FA and elevated MD and RD in parieto-occipital tracts, which are involved in sensory perception and multisensory integration (Chang et al., 2014). Notably, children with ASD – but not SPD – had impaired microstructure in temporal tracts involved in social-emotional processing compared to TDC (Chang et al., 2014). Using a larger study group with inclusion of direct measures of auditory and tactile processing in

Table 2

White matter tracks with significantly different DTI and tractography metrics between children with SPD and TDC on voxel-wise analysis.

	FA	MD	RD	TD	ED
Genu of corpus callosum	0	0	742	0	0
Body of corpus callosum	0	0	1808	1470	519
Splenium of corpus callosum	0	1	1746	2205	2289
Anterior corona radiata – Left	0	0	1477	0	0
Anterior corona radiata – Right	0	0	1207	0	495
Superior corona radiata – Left	0	0	859	286	0
Superior corona radiata – Right	0	0	778	0	538
Posterior corona radiata – Left	0	0	587	204	171
Posterior corona radiata – Right	0	49	610	422	511
Superior longitudinal fasciculus – Left	0	0	592	760	0
Superior longitudinal fasciculus – Right	0	15	644	0	1016
Anterior limb of internal capsule – Left	0	0	454	0	0
Anterior limb of internal capsule – Right	0	0	0	0	288
Posterior limb of internal capsule – Left	0	0	526	0	258
Posterior limb of internal capsule – Right	0	428	621	9	609
Retrolenticular part of internal capsule – Left	0	0	597	0	13
Retrolenticular part of internal capsule – Right	0	0	54	0	480
Posterior thalamic radiation – Left	0	0	870	140	158
Posterior thalamic radiation – Right	209	700	813	84	863
External capsule – Left	0	0	806	0	17
External capsule – Right	0	8	109	0	854
Cingulum – Left	0	0	126	0	3
Cingulum – Right	0	0	0	22	83
Fornix – Left	0	0	156	0	143
Fornix – Right	0	5	13	0	105
Cerebral peduncle – Left	0	0	324	0	9
Cerebral peduncle – Right	0	0	0	0	170
Tapetum – Left	0	0	12	24	24
Tapetum – Right	0	35	54	44	68
Sagittal stratum – Left	0	0	114	0	136
Sagittal stratum – Right	0	122	320	0	215

Each cell represents the number of voxels with significantly different DTI and/or tractography metrics between children with SPD and TDC on voxel-wise TBSS analysis after applying TFCE correction (p < .05, Fig. 1). Children with SPD had significantly lower FA, TD, and ED but higher MD and RD compared to TDC.

2015, Chang et al. reported reduced FA in bilateral posterior thalamic radiation and splenium of corpus callosum in children with SPD (Chang et al., 2015). It is also notable that some prior studies in ASD subjects have shown impaired microstructural integrity and reduced connectome ED in genu of corpus callosum (Nickel et al., 2017; Payabvash et al., 2019b); whereas, in our cohort of children with SPD, the microstructural and connectivity impairment was more striking in the splenium of corpus callosum. Our findings suggest a potential role for connectomic biomarkers to potentially differentiate children with SPD from those with ASD.

While conventional DTI metrics, such as FA, are sensitive to microstructural impairment, they do not include any information regarding the directionality of water molecule diffusion. TD applies the inherently high directional accuracy of diffusion fiber tractography to more directly estimate connectivity (Calamante et al., 2010, 2012a,b). The ED maps, on the other hand, represent the anatomic embedding of white matter connectomic edges (Owen et al., 2015). While, in TD maps, there is no constraint on the streamline tractography; in ED maps, parcellation of cortical and subcortical gray matter is applied to define connectome nodes, and to constrain streamline tracks to direct connections between pairs of connectome nodes (Owen et al., 2015). In normal brain white matter, the ED had negative correlation with neurite orientation dispersion, and positive correlation with neurite density and TD at voxel levels (Owen et al., 2015). Moreover, the ED was higher in posterior cerebral white matter than in anterior white matter, more strikingly so, compared to FA and TD differences (Owen et al., 2015). A disproportionately higher ED in posterior and periventricular white matter of the normal brain may lend itself to evaluation of disorders that preferentially affect these posterior and/or periventricular regions.
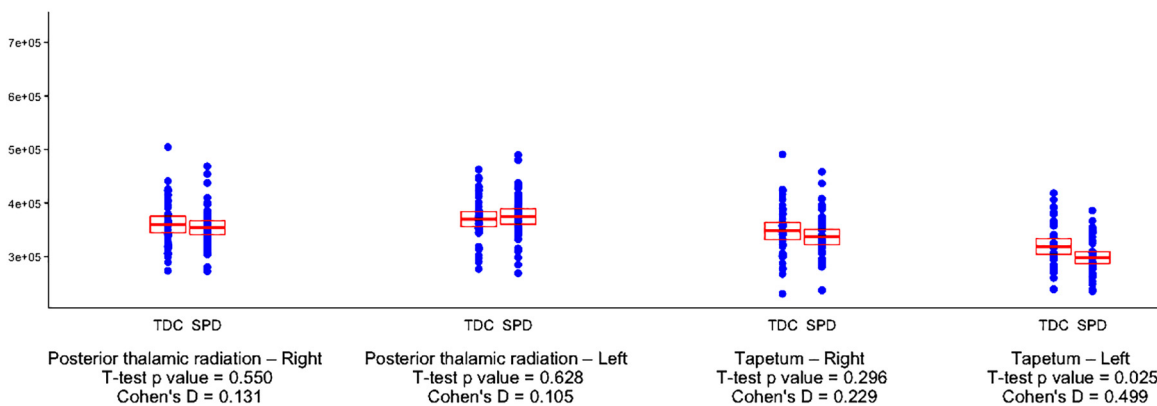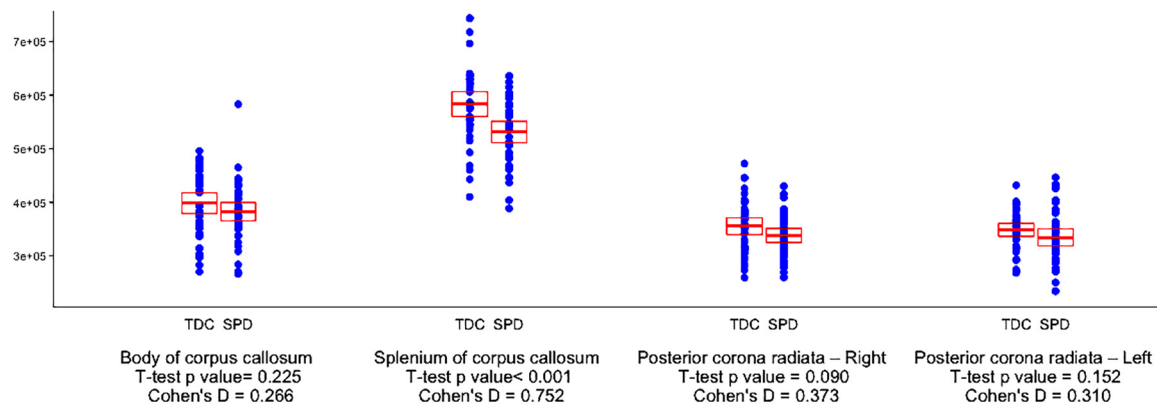
Our findings of diminished TD and ED in posterior white matter tracts imply reduced density of posterior projection and commissural neuronal fibers in children with SPD – notably in the absence of regional gray matter differences in VBM analysis. Thus, while the volume of gray matter may not be significantly different in children with SPD compared to control subjects, SPD was associated with reduced number of posterior commissural fibers traversing through the splenium of corpus callosum. Also, in multivariate stepwise penalized logistic regression analysis, the only independent variable distinguishing children with SPD from TDC was the average TD in the splenium of the corpus callosum. Penalized regression model offers a statistical solution for multivariate analysis with a high number of collinear predictors, and binary or ordinal dependent variables (Park and Hastie, 2008; Payabvash et al., 2017, 2018). In recent years, the penalized estimation methods have been proposed to stabilize the selection process in regression models, and to prevent data over-fit due to collinearity of the covariates or high-dimensionality (Frost et al., 2015; Park and Hastie, 2008). The penalized logistic regression analyses were originally applied for detecting gene-gene interactions (Park and Hastie, 2008), but recently became popular in image analysis in order to overcome the shortcomings of standard logistic regression analysis given the large number of adjacent voxels/regions in comparison to the small number of subjects (Teipel et al., 2015). Correction for collinearity of predictors was particularly crucial in our study since connectomic and diffusion metrics of adjacent white matter tracts tend to change in similar direction. Thus, applying penalized regression seems appropriate to identify the "independent" microstructural or connectivity predictor of SPD among a large number of tract-based variables that have significant differences between study groups in univariate analyses. Hence, among all connectomic/DTI variables, the average TD in the splenium of the corpus callosum can provide an independent predictor for SPD. These results point to the crucial role of splenial commissural neural fiber density in the neurobiological mechanism of SPD, implicating inter-hemispheric communication among sensory cortical areas. The splenium of the corpus callosum connects homotopic regions of the occipital, parietal, and temporal lobes, which mainly involve visual processing (Knyazeva, 2013). White matter microstructural dysintegrity in the splenium of patients with ASD were attributed to abnormalities of visual processing, such as face recognition processing (Hubl et al., 2003; Prywweler et al., 2014). With further validation in future studies, the splenial average TD potentially offers a quantitative biomarker for differentiating children with SPD from neurotypical controls. Such quantitative and objective measures can add value to the clinical interpretation of brain MRI scans in children with suspected neurodevelopmental disorders.
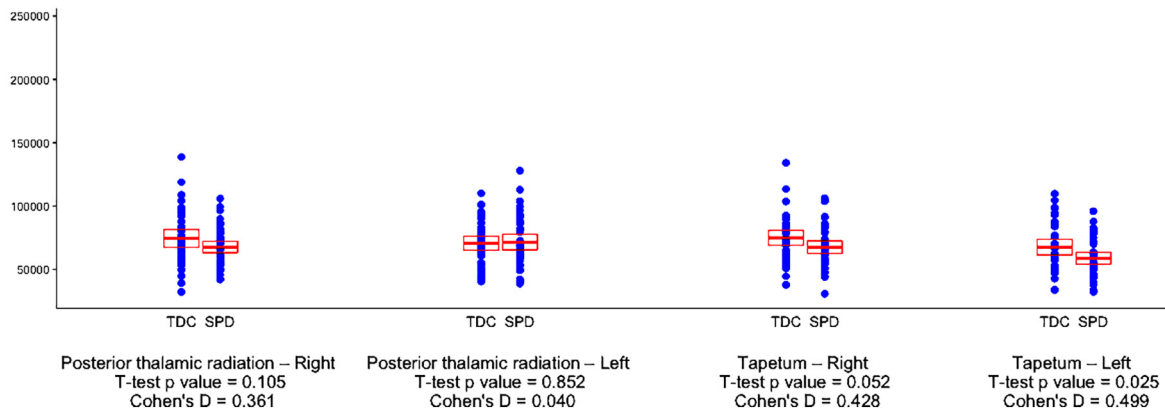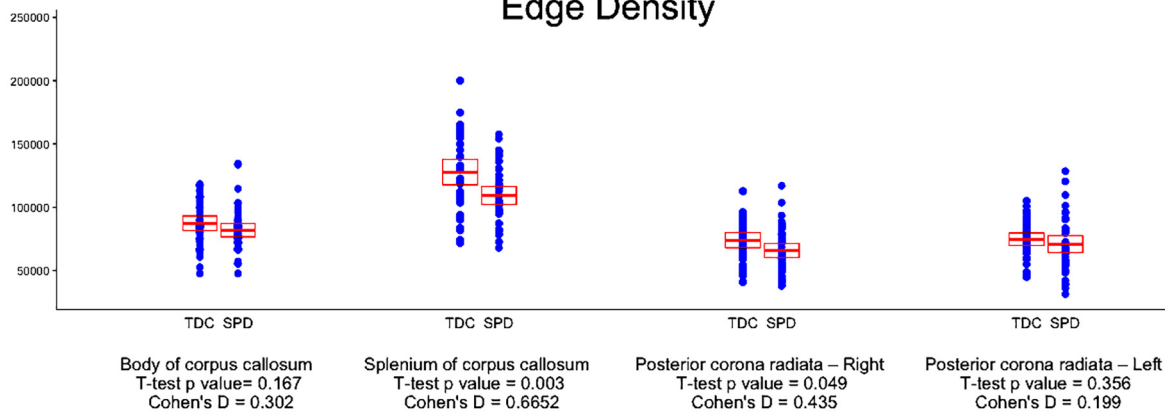
The machine learning algorithms are statistically well suited for multivariate analysis that account for the known inter-regional correlations of white matter microstructure (Li et al., 2012, 2017; Wahl et al., 2010). Using atlas-based regional DTI metrics and SVM algorithms, Jin et al. achieved an accuracy of 76% in classification of infants at high risk of ASD (Jin et al., 2015). Our study is the first in the literature applying machine learning algorithms for classification of children with SPD based on DTI microstructural and connectivity information. Given the relatively small population size, we opted to report the performance of different models after cross-validation among 500 randomly selected validation samples. Overall, tractography variables (i.e., TD and ED) applying random forest and naïve Bayes algorithms yielded greater accuracy and test performance than microstructural metrics (i.e., FA, MD, AD and RD), with the most accurate combination from random forest classification based on tract-based TD. While these findings should be confirmed in larger cohorts, our results suggest that future studies applying machine-learning models for classification of SPD should consider random-forest models and connectivity metrics (e.g. TD) in their prediction model.

Future studies can determine whether the machine-learning

Track Density

Body of corpus callosum
T-test p value= 0.225
Cohen's D = 0.266

Splenium of corpus callosum
T-test p value< 0.001
Cohen's D = 0.752

Posterior corona radiata – Right
T-test p value = 0.090
Cohen's D = 0.373

Posterior corona radiata – Left
T-test p value = 0.152
Cohen's D = 0.310

Posterior thalamic radiation – Right
T-test p value = 0.550
Cohen's D = 0.131

Posterior thalamic radiation – Left
T-test p value = 0.628
Cohen's D = 0.105

Tapetum – Right
T-test p value = 0.296
Cohen's D = 0.229

Tapetum – Left
T-test p value = 0.025
Cohen's D = 0.499

Edge Density

Body of corpus callosum
T-test p value= 0.167
Cohen's D = 0.302

Splenium of corpus callosum
T-test p value = 0.003
Cohen's D = 0.6652

Posterior corona radiata – Right
T-test p value = 0.049
Cohen's D = 0.435

Posterior corona radiata – Left
T-test p value = 0.356
Cohen's D = 0.199

Posterior thalamic radiation – Right
T-test p value = 0.105
Cohen's D = 0.361

Posterior thalamic radiation – Left
T-test p value = 0.852
Cohen's D = 0.040

Tapetum – Right
T-test p value = 0.052
Cohen's D = 0.428

Tapetum – Left
T-test p value = 0.025
Cohen's D = 0.499

(caption on next page)

Fig. 2. Scatterplot of track-based average TD and ED in 8 white matter tracks. For each white matter track, the children with SPD are on the right and TDC are on the left. The student *t*-test *p* values and effect size are reported for each white matter track. The boxplot represents the mean ± 95% confidence interval. Applying Bonferroni correction, the corrected p value for multiple comparison among 48 white matter tracts would be < 0.001.

algorithms can also help distinguish SPD from other neurodevelopmental disorders. Our results provide the first step in understanding the underlying connectomic correlates of SPD, and provide the preliminary results for methodological design of future machine learning classifiers. If in fact, the DTI/connectomic predictors of SPD are found to be similar to other conditions such as ASD, then it is probable that these condition present overlapping genetics and behavioral dysfunction, and this is compelling for moving the field towards understanding neurodevelopment as a broader concept with each child having a more unique subset based on their brain connectivity and function. Eventually, longitudinal follow-up studies can determine the trajectory of microstructural changes over time, or help determine the efficacy of treatment interventions.

Our findings should be interpreted in light of some limitations. Although the current study presents the largest imaging cohort with SPD, the sample size remains too small to draw firm conclusions about diagnostic accuracy. Moreover, children with SPD represent a heterogeneous cohort with sensory hyper- or hypo-responsivity, and tactile, auditory, and/or visual processing disorders. Future exploration of more specific sensory phenotypes, such as auditory over-responsivity, will further define our understanding of this heterogeneous condition. Another limitation in generalizability of these results is the restriction of participant age to 8 to 12 years – in an effort to reduce the confounding effect of subjects' age.

In conclusion, these findings reveal the white matter connectivity and connectomic correlates of SPD, with reduced TD and ED along

Fractional Anisotropy

	Accuracy	Sensitivity	Specificity	PPV	NPV
Naive Bayes	71%	63%	81%	78%	67%
Random forest	68%	70%	66%	72%	66%
SVM – linear kernel	61%	51%	72%	68%	58%
SVM – polynomial kernel	62%	58%	66%	67%	59%
Neural Network – single layer *	64%	58%	71%	70%	61%
Neural Network – double layers *	64%	60%	69%	70%	61%

Mean Diffusivity

	Accuracy	Sensitivity	Specificity	PPV	NPV
Naive Bayes	66%	58%	76%	72%	63%
Random forest	73%	73%	73%	77%	70%
SVM – linear kernel	62%	65%	58%	66%	59%
SVM – polynomial kernel	61%	63%	59%	65%	57%
Neural Network – single layer *	63%	66%	59%	66%	59%
Neural Network – double layers *	64%	68%	60%	69%	61%

Radial Diffusivity

	Accuracy	Sensitivity	Specificity	PPV	NPV
Naive Bayes	70%	61%	79%	77%	66%
Random forest	66%	69%	63%	70%	63%
SVM – linear kernel	61%	68%	54%	64%	57%
SVM – polynomial kernel	60%	66%	53%	63%	56%
Neural Network – single layer *	63%	69%	55%	66%	59%
Neural Network – double layers *	61%	65%	55%	64%	57%

Edge Density

	Accuracy	Sensitivity	Specificity	PPV	NPV
Naive Bayes	72%	73%	72%	77%	70%
Random forest	76%	76%	77%	81%	74%
SVM – linear kernel	72%	65%	80%	79%	69%
SVM – polynomial kernel	68%	68%	67%	71%	65%
Neural Network – single layer *	74%	72%	76%	80%	71%
Neural Network – double layers *	72%	71%	73%	78%	70%

Track Density

	Accuracy	Sensitivity	Specificity	PPV	NPV
Naive Bayes	72%	76%	68%	75%	71%
Random forest	78%	74%	82%	83%	75%
SVM – linear kernel	72%	62%	83%	80%	69%
SVM – polynomial kernel	64%	64%	65%	67%	63%
Neural Network – single layer *	70%	66%	75%	77%	67%
Neural Network – double layers *	70%	65%	74%	77%	66%

Color scale: 90%, 80%, 70%, 60%, 50%

Fig. 3. Heat map summary for classification performance of different machine learning algorithms using DTI and tractography metrics. The test characteristics (e.g. accuracy, sensitivity, …) were calculated in validation datasets from ×500 cross validation – details in Supplemental Table 1.
* The neural networks were designed to have one (single) or two (double) hidden layers.

posterior projection and commissural fiber tracts representing lower neural fiber density and connectome edge density, respectively, but without appreciable gray matter morphological changes. These white matter alterations may serve as a neurobiological marker of SPD. Indeed, the average TD in splenium of corpus callosum was the most distinctive DTI/tractography metric for identification of SPD, which can lend itself to a ROI-based quantitative measure for the diagnosis of children with SPD, and potentially add value to clinical interpretation of brain MRI in the pediatric population. Finally, we demonstrated the feasibility and accuracy of supervised machine learning algorithms in devising a classification biomarker for SPD with integration of a multitude of tract-based DTI and tractography metrics. These tools can potentially transform interpretation of clinical scans in children with suspected neurodevelopmental disorders by devising objective and quantitative measures for timely diagnosis based on microstructural and connectomic integrity along with the traditional visual macrostructural evaluation.

Author disclosure statement

There were no commercial associations to create a conflict of interest in connection with submitted manuscript.

Supplementary data to this article can be found online at https://doi.org/10.1016/j.nicl.2019.101831.

Acknowledgments

References

Ahn, R.R., Miller, L.J., Milberger, S., McIntosh, D.N., 2004. Prevalence of parents' perceptions of sensory processing disorders among kindergarten children. Am. J. Occup. Ther. 58, 287–293.

Ben-Sasson, A., Carter, A.S., Briggs-Gowan, M.J., 2009. Sensory over-responsivity in elementary school: prevalence and social-emotional correlates. J. Abnorm. Child Psychol. 37, 705–716.

Brandes-Aitken, A., Anguera, J.A., Rolle, C.E., Desai, S.S., Demopoulos, C., Skinner, S.N., Gazzaley, A., Marco, E.J., 2018. Characterizing cognitive and visuomotor control in children with sensory processing dysfunction and autism spectrum disorders. Neuropsychology 32, 148–160.

Bullmore, E., Sporns, O., 2009. Complex brain networks: graph theoretical analysis of structural and functional systems. Nat. Rev. Neurosci. 10, 186–198.

Calamante, F., Tournier, J.D., Jackson, G.D., Connelly, A., 2010. Track-density imaging (TDI): super-resolution white matter imaging using whole-brain track-density mapping. Neuroimage 53, 1233–1243.

Calamante, F., Tournier, J.D., Kurniawan, N.D., Yang, Z., Gyengesi, E., Galloway, G.J., Reutens, D.C., Connelly, A., 2012a. Super-resolution track-density imaging studies of mouse brain: comparison to histology. Neuroimage 59, 286–296.

Calamante, F., Tournier, J.D., Smith, R.E., Connelly, A., 2012b. A generalised framework for super-resolution track-weighted imaging. Neuroimage 59, 2494–2503.

Chang, Y.S., Owen, J.P., Desai, S.S., Hill, S.S., Arnett, A.B., Harris, J., Marco, E.J., Mukherjee, P., 2014. Autism and sensory processing disorders: shared white matter disruption in sensory pathways but divergent connectivity in social-emotional pathways. PLoS ONE 9, e103038.

Chang, Y.S., Gratiot, M., Owen, J.P., Brandes-Aitken, A., Desai, S.S., Hill, S.S., Arnett, A.B., Harris, J., Marco, E.J., Mukherjee, P., 2015. White matter microstructure is associated with auditory and tactile processing in children with and without sensory processing disorder. Front. Neuroanat. 9, 169.

Douaud, G., Smith, S., Jenkinson, M., Behrens, T., Johansen-Berg, H., Vickers, J., James, S., Voets, N., Watkins, K., Matthews, P.M., James, A., 2007. Anatomically related grey and white matter abnormalities in adolescent-onset schizophrenia. Brain 130, 2375–2386.

Frost, H.R., Andrew, A.S., Karagas, M.R., Moore, J.H., 2015. A screening-testing approach for detecting gene-environment interactions using sequential penalized and unpenalized multiple logistic regression. Pac. Symp. Biocomput. 183–194.

Greene, C.A., Cieslak, M., Grafton, S.T., 2017. Effect of different spatial normalization approaches on tractography and structural brain networks. Netw. Neurosci. 1–43.

Hubl, D., Bolte, S., Feineis-Matthews, S., Lanfermann, H., Federspiel, A., Strik, W., Poustka, F., Dierks, T., 2003. Functional imbalance of visual pathways indicates alternative face processing strategies in autism. Neurology 61, 1232–1237.

Jin, Y., Wee, C.Y., Shi, F., Thung, K.H., Ni, D., Yap, P.T., Shen, D., 2015. Identification of infants at high-risk for autism spectrum disorder using multiparameter ultiscale white matter connectivity networks. Hum. Brain Mapp. 36, 4880–4896.

Knyazeva, M.G., 2013. Splenium of corpus callosum: patterns of interhemispheric interaction in children and adults. Neural Plast. 2013, 639430.

Koziol, L.F., Budding, D., 2012. ADHD and sensory processing disorders: placing the diagnostic issues in context. Appl. Neuropsychol. Child 1, 137–144.

Li, Y.O., Yang, F.G., Nguyen, C.T., Cooper, S.R., LaHue, S.C., Venugopal, S., Mukherjee, P., 2012. Independent component analysis of DTI reveals multivariate microstructural correlations of white matter in the human brain. Hum. Brain Mapp. 33, 1431–1451.

Li, D., Karnath, H.O., Xu, X., 2017. Candidate biomarkers in children with autism Spectrum disorder: a review of MRI studies. Neurosci. Bull. 33, 219–237.

May-Benson, T.A., Koomar, J.A., Teasdale, A., 2009. Incidence of pre-, peri-, and postnatal birth and developmental problems of children with sensory processing disorder and children with autism spectrum disorder. Front. Integr. Neurosci. 3, 31.

Miller, L.J., Anzalone, M.E., Lane, S.J., Cermak, S.A., Osten, E.T., 2007. Concept evolution in sensory integration: a proposed nosology for diagnosis. Am. J. Occup. Ther. 61, 135–140.

Miller, L.J., Nielsen, D.M., Schoen, S.A., Brett-Green, B.A., 2009. Perspectives on sensory processing disorder: a call for translational research. Front. Integr. Neurosci. 3, 22.

Mitchell, A.W., Moore, E.M., Roberts, E.J., Hachtel, K.W., Brown, M.S., 2015. Sensory processing disorder in children ages birth-3 years born prematurely: a systematic review. Am. J. Occup. Ther. 69, 6901220030.

Mukherjee, P., Berman, J.I., Chung, S.W., Hess, C.P., Henry, R.G., 2008a. Diffusion tensor MR imaging and fiber tractography: theoretic underpinnings. AJNR Am. J. Neuroradiol. 29, 632–641.

Mukherjee, P., Chung, S.W., Berman, J.I., Hess, C.P., Henry, R.G., 2008b. Diffusion tensor MR imaging and fiber tractography: technical considerations. AJNR Am. J. Neuroradiol. 29, 843–852.

Nickel, K., Tebartz van Elst, L., Perlov, E., Endres, D., Muller, G.T., Riedel, A., Fangmeier, T., Maier, S., 2017. Altered white matter integrity in adults with autism spectrum disorder and an IQ > 100: a diffusion tensor imaging study. Acta Psychiatr. Scand. 135, 573–583.

Owen, J.P., Marco, E.J., Desai, S., Fourie, E., Harris, J., Hill, S.S., Arnett, A.B., Mukherjee, P., 2013. Abnormal white matter microstructure in children with sensory processing disorders. Neuroimage Clin. 2, 844–853.

Owen, J.P., Chang, Y.S., Mukherjee, P., 2015. Edge density imaging: mapping the anatomic embedding of the structural connectome within the white matter of the human brain. Neuroimage 109, 402–417.

Park, M.Y., Hastie, T., 2008. Penalized logistic regression for detecting gene interactions. Biostatistics 9, 30–50.

Parmar, C., Grossmann, P., Bussink, J., Lambin, P., Aerts, H.J.W.L., 2015. Machine learning methods for quantitative Radiomic biomarkers. Sci. Rep. 5, 13087.

Payabvash, S., Noorbaloochi, S., Qureshi, A.I., 2017. Topographic assessment of acute ischemic changes for prognostication of anterior circulation stroke. J. Neuroimaging 27, 227–231.

Payabvash, S., Benson, J.C., Tyan, A.E., Taleb, S., McKinney, A.M., 2018. Multivariate prognostic model of acute stroke combining admission infarct location and symptom severity: a proof-of-concept study. J. Stroke Cerebrovasc. Dis. 27, 936–944.

Payabvash, S., Palacios, E., Owen, J.P., Wang, M.B., Tavassoli, T., Gerdes, M.R., Brandes Aitken, A., Mukherjee, P., Marco, E.J., 2019a. White Matter Connectome Correlates of Auditory Over-Responsivity: Edge Density Imaging and Machine-Learning Classifiers. Front. Integr. Neurosci. 29, 10.

Payabvash, S., Palacios, E.M., Owen, J.P., Wang, M.B., Tavassoli, T., Gerdes, M., Brandes-Aitken, A., Cuneo, D., Marco, E.J., Mukherjee, P., 2019b. White matter connectome edge density in children with autism Spectrum disorders: potential imaging biomarkers using machine-learning models. Brain Connect. 9, 209–220.

Prywller, J.R., Schauder, K.B., Anderson, A.W., Heacock, J.L., Foss-Feig, J.H., Newsom, C.R., Loring, W.A., Cascio, C.J., 2014. White matter correlates of sensory processing in autism spectrum disorders. Neuroimage Clin. 6, 379–387.

Rutter, M., Bailey, A., Lord, C., 2003. Social Communication Questionnaire. WPS.

Smith, S.M., Jenkinson, M., Woolrich, M.W., Beckmann, C.F., Behrens, T.E., Johansen-Berg, H., Bannister, P.R., De Luca, M., Drobnjak, I., Flitney, D.E., Niazy, R.K., Saunders, J., Vickers, J., Zhang, Y., De Stefano, N., Brady, J.M., Matthews, P.M., 2004. Advances in functional and structural MR image analysis and implementation as FSL. Neuroimage 23, S208–S219 Suppl 1.

Teipel, S.J., Kurth, J., Krause, B., Grothe, M.J., Alzheimer's Disease Neuroimaging, I., 2015. The relative importance of imaging markers for the prediction of Alzheimer's disease dementia in mild cognitive impairment - beyond classical regression. Neuroimage Clin. 8, 583–593.

Tomchek, S.D., Dunn, W., 2007. Sensory processing in children with and without autism: a comparative study using the short sensory profile. Am. J. Occup. Ther. 61, 190–200.

Wahl, M., Li, Y.O., Ng, J., Lahue, S.C., Cooper, S.R., Sherr, E.H., Mukherjee, P., 2010. Microstructural correlations of white matter tracts in the human brain. Neuroimage 51, 531–541.